IEEE Access
Multidisciplinary | Rapid Review | Open Access Journal

Received February 17, 2021, accepted March 9, 2021, date of publication March 10, 2021, date of current version March 23, 2021.

Digital Object Identifier 10.1109/ACCESS.2021.3065500

Impacts of Nonlinear Energy Harvesting and Residual Self-Interference on the Performance of Full-Duplex Decode-and-Forward Relay System

BA CAO NGUYEN[1], TRAN MANH HOANG[2], LE THE DUNG[3], (Member, IEEE), AND TAEJOON KIM[3], (Member, IEEE)

[1]Faculty of Basic Techniques,Telecommunications University, Khanh Hoa 650000, Vietnam
[2]Faculty of Telecommunications Services, Telecommunications University, Khanh Hoa 650000, Vietnam
[3]School of Information and Communication Engineering, Chungbuk National University, Cheongju 28644, South Korea

Corresponding author: Taejoon Kim (ktjcc@chungbuk.ac.kr)

This work was supported by the Basic Science Research Program through the National Research Foundation of Korea (NRF), Ministry of Education under Grant 2020R1I1A3068305.

ABSTRACT In this paper, we investigate the usage of a nonlinear energy harvester at a full-duplex (FD) relay, which can harvest the energy from radio frequency (RF) signals transmitted from the source. We mathematically derive the exact closed-form expressions of outage probability (OP), throughput, and average symbol error rate (ASER) of the nonlinear energy harvester-wireless information and power transfer-FD relaying (N-WIPT-FDR) system over Rayleigh fading channels. Unlike linear energy harvester, nonlinear energy harvester results in more computational complexity. Furthermore, it makes the outage floor happen faster even when self-interference cancellation (SIC) techniques are effectively applied due to the saturation power threshold of the nonlinear energy harvester. The combination of nonlinear energy harvester characteristic and residual self-interference (RSI) has significant impacts on the OP, throughput, and ASER of the considered N-WIPT-FDR system. On the other hand, there is an optimal energy harvesting (EH) time duration, which minimizes the OP. This optimal value depends on the transmission power of the source and the saturation power threshold of the nonlinear energy harvester. Monte-Carlo simulations are conducted to validate the derived mathematical expressions.

INDEX TERMS Nonlinear energy harvesting, full-duplex relay, self-interference cancellation, decode-and-forward, outage probability, throughput, average symbol error rate.

I. INTRODUCTION

In recent years, green communication has emerged as a promising technique for future wireless networks such as the fifth-generation (5G) and beyond [1]. In green communication-oriented systems, various energy efficiency solutions such as using the low power consumption devices, radio frequency (RF) energy harvesting (EH), and sleep mode are applied to save the energy consumption [1], [2]. Among those, RF-EH has become a reality with the appearance of some commercial products and standards [3]. Therefore, exploiting the RF-EH technique to prolong the operation lifetime of wireless devices has been popular in both researches and experiments as energy and information can be simultaneously transmitted and received through RF signals [4].

Besides the RF-EH technique, the in-band full-duplex (FD) transmission technique is a new transmission method that has been recently proposed for wireless communication systems to solve the issue of lacking wireless spectrum. Compared with the traditional half-duplex (HD) transmission, FD transmission can double the spectral efficiency because FD devices can simultaneously transmit and receive signals at the same time and on the same frequency band [5]–[7]. However, a major issue of FD transmission is the self-interference (SI) from the transmitting antenna to the receiving antenna of FD device. Fortunately, recent studies and experiments have reported that the SI can be reduced up to 110 dB by using several self-interference cancellation (SIC) solutions such

The associate editor coordinating the review of this manuscript and approving it for publication was Deyu Zhang.

antenna designs, analog and digital signal processing [8], [9]. When effective SIC solutions are deployed so that FD devices can successfully decode the desired signal from the received signals.

Combining wireless information and power transfer (WIPT) and FD techniques into wireless communication systems with FD relay has been considered in many works such as [10]–[18]. In WIPT-FD relaying (FDR) systems, either relay harvests the energy from source [11], [13], [14], [16] or both source and relay harvest the energy from power beacon (PB) [12], [15], [17]. In these works, the closed-form expressions of outage probability (OP), throughput, symbol error probability (SEP), and ergodic capacity were derived, taking into account the impacts of various parameters such as residual self-interference (RSI), EH time duration, and data transmission rate [12], [14], [15], [17]. Their results demonstrated that the RSI significantly impacts the OP and SEP of WIPT-FDR systems. Notably, although linear energy harvester is used at FD relay, the OP and SEP reach the floors in high signal-to-noise ratio (SNR) due to the RSI. Furthermore, the optimal EH time duration can improve the throughput of WIPT-FDR systems compared with traditional WIPT-HDR systems [14].

Many methods have been proposed to enhance the throughput, OP, and SEP performance of WIPT-FDR systems. Specifically, in [10], a new throughput-oriented scheduling scheme was developed for a WIPT-FDR system with multiple users over Rician fading channels. It was shown that the proposed throughput-oriented scheduling scheme could help the WIPT-FDR system reach the highest throughput. A WIPT-FDR system with spatial modulation (SM) and physical-layer network coding was investigated in [18]. The authors showed that the bit-error-rate (BER) performance of the FD-SM system could be better than that of the conventional HD-SM system if the quality of SIC is enhanced, and the spectral efficiency requirement increases. The authors of [16] proposed an optimization problem with a non-convex form to minimize the power consumption of FD secure communications in cellular networks with downlink WIPT. It was demonstrated that the proposed FD secure scheme is more power-efficient than the conventional one.

Recently, besides mathematical analysis, optimization methods and experimental measurements have been introduced to improve the performance of WIPT-FDR systems [19]–[23]. By optimizing the time switching (TS) ratio in WIPT-FDR systems, the OP is significantly reduced and the throughput is greatly enhanced. On the other hand, nonlinear energy harvester was been investigated in WIPT-FDR systems [24], [25]. Specifically, in the that closed-form expression for optimal TS cannot be achieved due to the complexity in calculation, some useful methods can be applied to increase the throughput and energy efficiency of WIPT-FDR systems [24]. In addition, beamforming is a good solution to improve the amount of harvested energy at FDR [25].

As discussed above, there have been many works investigating the benefits of both EH and FD techniques in WIPT-FDR systems through mathematical analyses or simulations. Although linear energy harvester has been widely used in the literature, recent reports such as [26]–[29] demonstrated that it might be impractical. In fact, there are various factors causing the nonlinear characteristic of energy harvester such as diode and saturation nonlinearities. Nonlinearity is the intrinsic property of diode. Meanwhile, the saturation nonlinearities were confirmed by experiments on energy harvesting circuits [3]. Therefore, the output power of energy harvester in practice is often a nonlinear function of the amount of harvested energy. Specifically, the recent reports in [30], [31] demonstrated that nonlinear energy harvester caused saturated floor even for half-duplex relay (HDR) systems. In addition, the spectral efficiency and energy efficiency of nonlinear energy harvesting systems could be improved by optimizing the time switching ratio [30] and the bit error probability could be reduced via cooperative communications [31]. However, various scenarios using nonlinear energy harvester in wireless communication systems have not still been investigated, especially in terms of mathematical analysis. Motivated by this observation, in this paper, we exploit nonlinear energy harvester at the FD relay of a WIPT-FDR system (hereafter referred to as N-WIPT-FDR system). The contributions of this paper are as follows:

- We investigate a wireless relaying system where new techniques for future wireless networks such as energy harvesting, full-duplex transmission are applied. We observe that the usage of nonlinear energy harvester makes mathematical analysis much more complex in comparison with that in the case of using linear energy harvester. Consequently, most of previous works often derived expression of only one metric such as OP or throughput.
- We calculate the exact signal-to-interference-plus-noise ratio (SINR) of the considered N-WIPT-FDR system under the effect of the saturation power threshold of nonlinear energy harvester and the RSI induced by FD transmission. Based on this result, we successfully derive the exact closed-form expressions of the OP, throughput, and average symbol error rate (ASER) of the considered N-WIPT-FDR system over Rayleigh fading channels. From these expressions, we can easily derive the OP, throughput and ASER expressions of other relevant systems such as linear WIPT-FDR (L-WIPT-FDR) system by setting the saturation power threshold to extremely large value, N-WIPT-HD relay (HDR) system and L-WIPT-HDR system by setting RSI equals to zero and two time slots for signal transmissions, i.e., source to relay and relay to destination. All analysis expressions are validated by Monte-Carlo simulations.
- Based on the derived expressions, the performance of the considered N-WIPT-FDR system is investigated intensively. Numerical results indicate that the saturation power threshold causes the floor of OP, ASER even when the RSI is small. Moreover, the joint impact of the saturation power threshold and the RSI significantly

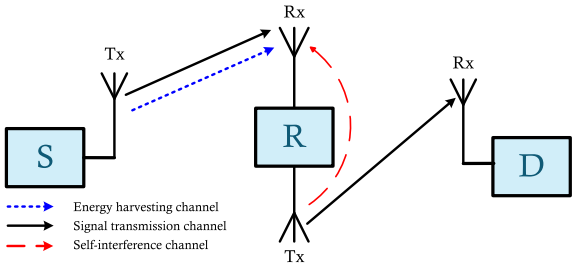

FIGURE 1. Block diagram of the considered N-WIPT-FDR system.

affects the OP, throughput, and ASER of the considered system. Specifically, the throughput cannot reach the target value due to the influences of the saturation power threshold, RSI, and time switching ratio. On the other hand, there is an optimal time switching ratio that minimizes the OP, ASER and maximizes the throughput. This value depends on the transmission power of the source, the saturation power threshold, and the RSI.

The rest of this paper is organized as follows. Section II presents in detail the system and signal models of the considered N-WIPT-FDR system. Section III mathematically derives the exact closed-form expressions of OP and throughput of the considered system. Section IV provides several numerical results obtained from these derived expressions. Finally, Section V concludes the paper.

II. SYSTEM MODEL

Fig. 1 demonstrates the system model of the considered N-WIPT-FDR system where the source (S) and destination (D) are single-antenna devices operating in half-duplex (HD) mode while relay (R) is a double-antenna device operating in FD mode. One antenna of R is used for transmitting signals, and the other is used for receiving signals. Additionally, since R employs a nonlinear energy harvester to harvest the energy from RF signals transmitted from S, the transmission power of R only depends on the transmission power of S up to a certain saturation power threshold of the energy harvester [27]. Notice that in the relay systems, amplified-and-forward (AF) and decode-and-forward (DF) are two popular relaying protocols. Although AF protocol is simpler than DF protocol, DF relay can achieve better performance in comparison to that of AF relay [32]. In this paper, the considered N-WIPT-FDR system are effected by various negative factors such as the RSI and the saturation power threshold. Therefore, we choose DF protocol for our analysis.

The operation of the considered N-WIPT-FDR system lasts in two separate time durations, as illustrated in Fig. 2. The first time duration of αT is used for EH. The second time duration of $(1-\alpha)T$ is used for information transmission, where α and T are respectively the time switching ratio and the transmission block duration. Since R receives signals from S and simultaneously transmits signals to D, the SI from the transmitting antenna and to the receiving antennas of R appears. It should be noted that in realistic scenarios,

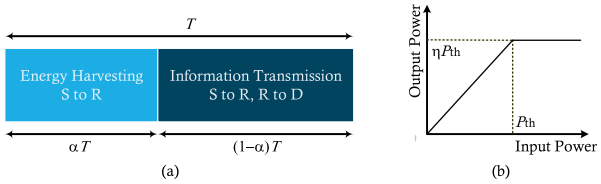

FIGURE 2. (a) Two time durations used in the considered N-WIPT-FDR system, (b) The relation between the input power and the output power of the relay equipped with nonlinear energy harvester.

R can use a shared antenna for both transmitting and receiving signals. However, using separate antennas for transmitting and receiving such as in the considered N-WIPT-FDR system significantly enhances the efficiency of SIC at FD devices because various solutions for SIC in antenna domain such as isolation, antenna directionality, and cross-polarization can be easily deployed for separate antennas [6], [9], [33].

In the EH time duration αT, the harvested energy at R with nonlinear energy harvester (denoted by $E_{\rm NEH}$) is computed as [27]

$$E_{\rm NEH} = \begin{cases} \eta\alpha T P_{\rm S}|h_{\rm SR}|^2, & P_{\rm S}|h_{\rm SR}|^2 \le P_{\rm th} \\ \eta\alpha T P_{\rm th}, & P_{\rm S}|h_{\rm SR}|^2 > P_{\rm th} \end{cases} \quad (1)$$

where η, $0 \leqslant \eta \leqslant 1$, is the energy conversion efficiency of the nonlinear energy harvester; $P_{\rm S}$ is the average transmission power of S; $h_{\rm SR}$ is the channel from the transmitting antenna of S to the receiving antenna of R; $P_{\rm th}$ is the saturation power threshold.

Next, R uses all harvested energy for forwarding data. Mathematically, the transmission power of R used in the time duration $(1-\alpha)T$ is given by

$$P_{\rm R} = \frac{E_{\rm NEH}}{(1-\alpha)T} = \begin{cases} \frac{\eta\alpha P_{\rm S}|h_{\rm SR}|^2}{1-\alpha}, & P_{\rm S}|h_{\rm SR}|^2 \le P_{\rm th}, \\ \frac{\eta\alpha P_{\rm th}}{1-\alpha}, & P_{\rm S}|h_{\rm SR}|^2 > P_{\rm th}. \end{cases} \quad (2)$$

During $(1-\alpha)T$, since R simultaneously transmits and receives signals simultaneously and on the same frequency band, the SI appears. Therefore, the received signal at R is expressed as

$$y_{\rm R} = h_{\rm SR}\sqrt{P_{\rm S}}x_{\rm S} + \tilde{h}_{\rm RR}\sqrt{P_{\rm R}}x_{\rm R} + n_{\rm R}, \quad (3)$$

where $x_{\rm S}$ and $x_{\rm R}$ are the transmitted signals of S and R, respectively; $P_{\rm R}$ is the average transmission power of R; $\tilde{h}_{\rm RR}$ is the SI channel from the transmitting antenna to the receiving antenna of R; $n_{\rm R}$ is the Gaussian noise with zero mean and variance of $\sigma_{\rm R}^2$, i.e., $n_{\rm R} \sim \mathcal{CN}(0, \sigma_{\rm R}^2)$.

It is obvious from (3) that, the average SI power is calculated as $\mathbb{E}\{|\tilde{h}_{\rm RR}|^2\}P_{\rm R}$, where $\mathbb{E}$ is the expectation operator. This SI power may be much higher than the power of desired signals. Thus, we should apply all SIC techniques at R to decrease the SI power. Specifically, several solutions in antenna domain such as cross-polarization, antenna directionality, and isolation are used first. Thanks to the usage of separate antennas, these solutions in the antenna domain can effectively reduce the SI power up to 30 dB [8], [9]. Then, the SI suppression in analog and digital domains is

carried out by using suitable circuits and algorithms. These techniques can mitigate SI up to 50 dB in the analog domain and 60 dB in the digital domain [8], [33], [34]. Overall, after applying all SIC methods, FD devices can cancel the SI up to 110 dB [8], [33], [34], making FD communication systems become feasibly in realistic scenarios. On the other hand, the residual self-interference (RSI) after all SIC techniques (denoted by $I_{\rm R}$) become Gaussian variable with zero mean and variance of $\gamma_{\rm RSI}$ [35]–[37], where $\gamma_{\rm RSI}$ is

$$\gamma_{\rm RSI} = \begin{cases} \frac{k\eta\alpha P_{\rm S}}{1-\alpha}, & P_{\rm S} \le P_{\rm th}, \\ \frac{k\eta\alpha P_{\rm th}}{1-\alpha}, & P_{\rm S} > P_{\rm th}, \end{cases} \tag{4}$$

with k is the RSI level due to imperfect SIC.

Now, the received signal at R can be rewritten as

$$y_{\rm R} = h_{\rm SR}\sqrt{P_{\rm S}}x_{\rm S} + I_{\rm R} + n_{\rm R}. \tag{5}$$

Then, R decodes the received signal and recodes this signal for forwarding. The received signals at D is presented as

$$y_{\rm D} = h_{\rm RD}\sqrt{P_{\rm R}}x_{\rm R} + n_{\rm D}, \tag{6}$$

where $h_{\rm RD}$ is the channel from the transmitting antenna of R to the receiving antenna of D; $n_{\rm D} \sim \mathcal{CN}(0, \sigma_{\rm D}^2)$ is the Gaussian noise at D.

From (5) and (6), the SINRs at R and D are, respectively, calculated as

$$\gamma_{\rm R} = \frac{|h_{\rm SR}|^2 P_{\rm S}}{\gamma_{\rm RSI} + \sigma_{\rm R}^2} = \Phi|h_{\rm SR}|^2, \tag{7}$$

$$\gamma_{\rm D} = \frac{|h_{\rm RD}|^2 P_{\rm R}}{\sigma_{\rm D}^2} = \begin{cases} \frac{\eta\alpha P_{\rm S}|h_{\rm SR}|^2|h_{\rm RD}|^2}{\sigma_{\rm D}^2(1-\alpha)}, & P_{\rm S}|h_{\rm SR}|^2 \le P_{\rm th} \\ \frac{\eta\alpha P_{\rm th}|h_{\rm RD}|^2}{\sigma_{\rm D}^2(1-\alpha)}, & P_{\rm S}|h_{\rm SR}|^2 > P_{\rm th} \end{cases} = \begin{cases} \Psi|h_{\rm SR}|^2|h_{\rm RD}|^2, & P_{\rm S}|h_{\rm SR}|^2 \le P_{\rm th} \\ \Theta|h_{\rm RD}|^2, & P_{\rm S}|h_{\rm SR}|^2 > P_{\rm th}. \end{cases} \tag{8}$$

where $\Phi = \frac{P_{\rm S}}{\gamma_{\rm RSI}+\sigma_{\rm R}^2}$, $\Psi = \frac{\eta\alpha P_{\rm S}}{\sigma_{\rm D}^2(1-\alpha)}$, and $\Theta = \frac{\eta\alpha P_{\rm th}}{\sigma_{\rm D}^2(1-\alpha)}$.

III. PERFORMANCE ANALYSIS

A. OUTAGE PROBABILITY

In this subsection, we mathematically derive the closed-form expression of the OP of the considered N-WIPT-FDR system. The OP is defined as the probability that the instantaneous data transmission rate of the considered N-WIPT-FDR system is lower than a pre-data transmission rate. Since a time duration αT is used for EH, the OP is given by

$$\begin{aligned} \text{OP} &= \Pr\{(1-\alpha)\log_2(1+\gamma_{\rm e2e}) < \mathcal{R}\} \\ &= \Pr\{\gamma_{\rm e2e} < 2^{\frac{\mathcal{R}}{1-\alpha}} - 1\}, \end{aligned} \tag{9}$$

where $\gamma_{\rm e2e}$ and $\mathcal{R}$ are respectively the end-to-end SINR and pre-data transmission rate. Since the DF protocol is deployed at FD relay, $\gamma_{\rm e2e}$ is expressed as

$$\gamma_{\rm e2e} = \min\{\gamma_{\rm R}, \gamma_{\rm D}\}, \tag{10}$$

where $\gamma_{\rm R}$ and $\gamma_{\rm D}$ are respectively given by (7) and (8).

Let $\gamma_{\rm th} = 2^{\frac{\mathcal{R}}{1-\alpha}} - 1$ be the SINR threshold. Then, (9) becomes

$$\text{OP} = \Pr\{\gamma_{\rm e2e} < \gamma_{\rm th}\}. \tag{11}$$

Combining of (10) and (11), we can see that the outage occurs when the received SINRs at R ($\gamma_{\rm R}$) or D ($\gamma_{\rm D}$) falls below a threshold $\gamma_{\rm th}$. Mathematically, (11) can be rewritten as

$$\text{OP} = \Pr\{\gamma_{\rm R} < \gamma_{\rm th}\} + \Pr\{\gamma_{\rm R} \ge \gamma_{\rm th}, \gamma_{\rm D} < \gamma_{\rm th}\}. \tag{12}$$

Replacing $\gamma_{\rm R}$ and $\gamma_{\rm D}$ in (7) and (8) into (12), we can present (12) as

$$\begin{aligned} \text{OP} = &\underbrace{\Pr\{\Phi|h_{\rm SR}|^2 < \gamma_{\rm th}\}}_{J_1} \\ &+ \underbrace{\Pr\{\Phi|h_{\rm SR}|^2 \ge \gamma_{\rm th}, \Psi|h_{\rm SR}|^2|h_{\rm RD}|^2 < \gamma_{\rm th}, \Theta|h_{\rm RD}|^2 \ge \gamma_{\rm th}\}}_{J_2} \\ &+ \underbrace{\Pr\{\Phi|h_{\rm SR}|^2 \ge \gamma_{\rm th}, \Theta|h_{\rm RD}|^2 < \gamma_{\rm th}\}}_{J_3}. \end{aligned} \tag{13}$$

Based on (13), the OP of the considered N-WIPT-FDR system is derived in the following Theorem 1.

Theorem 1: The exact closed-form expression of the OP of the considered N-WIPT-FDR system is computed as in (14), as shown at the bottom of the page, where $\Omega_1 = \mathbb{E}\{|h_{\rm SR}|^2\}$ and $\Omega_2 = \mathbb{E}\{|h_{\rm RD}|^2\}$ are respectively the average gains of S – R and R – D channels; $\phi_n = \cos\left(\frac{(2n-1)\pi}{2N}\right)$; $u = \frac{1}{2}\left[\left(\frac{\Theta}{\Psi} - \frac{\gamma_{\rm th}}{\Phi}\right)\phi_n + \frac{\Theta}{\Psi} + \frac{\gamma_{\rm th}}{\Phi}\right]$; N is the complexity-accuracy trade-off parameter [38].

Proof: To derive the OP expression of the considered N-WIPT-FDR system, we need to compute three probabilities J_1, J_2, and J_3 in (13). For the convenience in calculating these probabilities, we firstly derive the cumulative distribution function (CDF, denoted by $F(.)$), and the probability density function (PDF, denoted by $f(.)$) of the instantaneous average channel gain $|h|^2$ (i.e., $|h_{\rm SR}|^2$ and $|h_{\rm RD}|^2$ in this paper) which follows Rayleigh fading distribution. The PDF and CDF of $|h|^2$ are given by

$$F_{|h|^2}(x) = \Pr\{|h|^2 < x\} = 1 - \exp\left(-\frac{x}{\Omega}\right), x \ge 0, \tag{15}$$

$$f_{|h|^2}(x) = \frac{1}{\Omega}\exp\left(-\frac{x}{\Omega}\right), x \ge 0. \tag{16}$$

where $\Omega = \mathbb{E}\{|h|^2\}$ is the average channel gain.

$$\text{OP} = \begin{cases} 1 - \exp\left(-\frac{\gamma_{\rm th}}{\Phi\Omega_1} - \frac{\gamma_{\rm th}}{\Theta\Omega_2}\right), & \gamma_{\rm th} > \frac{\Phi\Theta}{\Psi}, \\ 1 - \exp\left(-\frac{\Theta}{\Psi\Omega_1} - \frac{\gamma_{\rm th}}{\Theta\Omega_2}\right) - \frac{\pi}{2N\Omega_1}\left(\frac{\Theta}{\Psi} - \frac{\gamma_{\rm th}}{\Phi}\right)\sum_{n=1}^{N}\sqrt{1-\phi_n^2}\exp\left(-\frac{u}{\Omega_1} - \frac{\gamma_{\rm th}}{\Psi\Omega_2\, u}\right), & \gamma_{\rm th} \le \frac{\Phi\Theta}{\Psi}, \end{cases} \tag{14}$$

Now, the probability J_1 is calculated as

$$J_1 = \Pr\{\Phi|h_{\rm SR}|^2 < \gamma_{\rm th}\} = \Pr\{|h_{\rm SR}|^2 < \frac{\gamma_{\rm th}}{\Phi}\} = 1 - \exp\Big(-\frac{\gamma_{\rm th}}{\Phi\Omega_1}\Big). \quad (17)$$

Similarly, we compute J_2 as

$$J_2 = \Pr\{\Phi|h_{\rm SR}|^2 \geq \gamma_{\rm th}, \Psi|h_{\rm SR}|^2|h_{\rm RD}|^2 < \gamma_{\rm th}, \Theta|h_{\rm RD}|^2 \geq \gamma_{\rm th}\} = \Pr\left\{|h_{\rm SR}|^2 \geq \frac{\gamma_{\rm th}}{\Phi}, \frac{\gamma_{\rm th}}{\Theta} \leq |h_{\rm RD}|^2 < \frac{\gamma_{\rm th}}{\Psi|h_{\rm SR}|^2}\right\}. \quad (18)$$

To calculate J_2 in (18), we consider two cases, i.e., $\gamma_{\rm th} > \frac{\Phi\Theta}{\Psi}$ and $\gamma_{\rm th} \leq \frac{\Phi\Theta}{\Psi}$.

For the first case, the expression $\gamma_{\rm th} > \frac{\Phi\Theta}{\Psi}$ is equivalent to $\frac{\gamma_{\rm th}}{\Phi} > \frac{\Theta}{\Psi}$. From the definitions of Φ, Θ and Ψ after (8), we have $\frac{\Theta}{\Psi} = \frac{P_{\rm th}}{P_{\rm S}}$. Therefore, $\frac{\gamma_{\rm th}}{\Phi} > \frac{\Theta}{\Psi}$ becomes $\frac{\gamma_{\rm th}}{\Phi} > \frac{P_{\rm th}}{P_{\rm S}}$. Based on this result and the condition $|h_{\rm SR}|^2 \geq \frac{\gamma_{\rm th}}{\Phi}$, we obtain $|h_{\rm SR}|^2 \geq \frac{\gamma_{\rm th}}{\Phi} > \frac{P_{\rm th}}{P_{\rm S}}$. This expression is equivalent to $|h_{\rm SR}|^2 P_{\rm S} > P_{\rm th}$. Notice that the expression $|h_{\rm SR}|^2 P_{\rm S} > P_{\rm th}$ is the second condition in (8). When this condition is satisfied, the SINR at D is $\gamma_{\rm D} = \Theta|h_{\rm RD}|^2$, not $\Psi|h_{\rm SR}|^2|h_{\rm RD}|^2$. Therefore, we have $\Pr\{\Psi|h_{\rm SR}|^2|h_{\rm RD}|^2 < \gamma_{\rm th}\} = 0$, leading to $J_2 = 0$.

For the second case $\gamma_{\rm th} \leq \frac{\Phi\Theta}{\Psi}$, by applying similar methods above, we obtain $\frac{\gamma_{\rm th}}{\Phi} \leq |h_{\rm SR}|^2 \leq \frac{\Theta}{\Psi}$. Therefore, (18) can be rewritten as

$$J_2 = \Pr\left\{\frac{\gamma_{\rm th}}{\Phi} \leq |h_{\rm SR}|^2 \leq \frac{\Theta}{\Psi}, \frac{\gamma_{\rm th}}{\Theta} \leq |h_{\rm RD}|^2 < \frac{\gamma_{\rm th}}{\Psi|h_{\rm SR}|^2}\right\}. \quad (19)$$

Using the PDF expression in (16) for $|h_{\rm SR}|^2$ and $|h_{\rm RD}|^2$, we have

$$J_2 = \int_{\frac{\gamma_{\rm th}}{\Phi}}^{\frac{\Theta}{\Psi}} \frac{1}{\Omega_1}\exp\Big(-\frac{x}{\Omega_1}\Big)dx \int_{\frac{\gamma_{\rm th}}{\Theta}}^{\frac{\gamma_{\rm th}}{\Psi x}} \frac{1}{\Omega_2}\exp\Big(-\frac{y}{\Omega_2}\Big)dy. \quad (20)$$

The second integral in (20) can be easily solved, i.e.,

$$\int_{\frac{\gamma_{\rm th}}{\Theta}}^{\frac{\gamma_{\rm th}}{\Psi x}} \frac{1}{\Omega_2}\exp\Big(-\frac{y}{\Omega_2}\Big)dy = \exp\Big(-\frac{\gamma_{\rm th}}{\Theta\Omega_2}\Big) - \exp\Big(-\frac{\gamma_{\rm th}}{\Psi\Omega_2 x}\Big). \quad (21)$$

Then, J_2 becomes

$$J_2 = \frac{1}{\Omega_1}\int_{\frac{\gamma_{\rm th}}{\Phi}}^{\frac{\Theta}{\Psi}} \exp\Big(-\frac{x}{\Omega_1} - \frac{\gamma_{\rm th}}{\Theta\Omega_2}\Big)dx - \frac{1}{\Omega_1}\int_{\frac{\gamma_{\rm th}}{\Phi}}^{\frac{\Theta}{\Psi}} \exp\Big(-\frac{x}{\Omega_1} - \frac{\gamma_{\rm th}}{\Psi\Omega_2 x}\Big)dx. \quad (22)$$

The first integral in (22) can be simply computed as

$$\frac{1}{\Omega_1}\int_{\frac{\gamma_{\rm th}}{\Phi}}^{\frac{\Theta}{\Psi}} \exp\Big(-\frac{x}{\Omega_1} - \frac{\gamma_{\rm th}}{\Theta\Omega_2}\Big)dx = \exp\Big(-\frac{\gamma_{\rm th}}{\Phi\Omega_1} - \frac{\gamma_{\rm th}}{\Theta\Omega_2}\Big) - \exp\Big(-\frac{\Theta}{\Psi\Omega_1} - \frac{\gamma_{\rm th}}{\Theta\Omega_2}\Big). \quad (23)$$

For the second integral in (22), applying [38, Eq. (25.4.30)], we have

$$\begin{aligned}
&\frac{1}{\Omega_1}\int_{\frac{\gamma_{\rm th}}{\Phi}}^{\frac{\Theta}{\Psi}} \exp\Big(-\frac{x}{\Omega_1} - \frac{\gamma_{\rm th}}{\Psi\Omega_2 x}\Big)dx \\
&= \frac{\pi}{2N\Omega_1}\Big(\frac{\Theta}{\Psi} - \frac{\gamma_{\rm th}}{\Phi}\Big)\sum_{n=1}^{N}\sqrt{1-\phi_n^2} \\
&\quad \times \exp\Big(-\frac{1}{2\Omega_1}\Big[\Big(\frac{\Theta}{\Psi} - \frac{\gamma_{\rm th}}{\Phi}\Big)\phi_n + \frac{\Theta}{\Psi} + \frac{\gamma_{\rm th}}{\Phi}\Big]\Big) \\
&\quad \times \exp\Big(-\frac{\gamma_{\rm th}}{\frac{1}{2}\Psi\Omega_2\Big[\Big(\frac{\Theta}{\Psi} - \frac{\gamma_{\rm th}}{\Phi}\Big)\phi_n + \frac{\Theta}{\Psi} + \frac{\gamma_{\rm th}}{\Phi}\Big]}\Big) \\
&= \frac{\pi}{2N\Omega_1}\Big(\frac{\Theta}{\Psi} - \frac{\gamma_{\rm th}}{\Phi}\Big)\sum_{n=1}^{N}\sqrt{1-\phi_n^2}\exp\Big(-\frac{u}{\Omega_1} - \frac{\gamma_{\rm th}}{\Psi\Omega_2 u}\Big),
\end{aligned} \quad (24)$$

where u, N, ϕ_n are defined in Theorem 1.

Finally, we obtain J_2 in (25), shown on the bottom of next page.

Since two random variables in J_3, i.e., $|h_{\rm SR}|^2$ and $|h_{\rm RD}|^2$, are independent, the integral J_3 is now calculated as

$$\begin{aligned}
J_3 &= \Pr\{\Phi|h_{\rm SR}|^2 \geq \gamma_{\rm th}, \Theta|h_{\rm RD}|^2 < \gamma_{\rm th}\} \\
&= \Big(1 - \Pr\Big\{|h_{\rm SR}|^2 \leq \frac{\gamma_{\rm th}}{\Phi}\Big\}\Big)\Pr\Big\{|h_{\rm RD}|^2 < \frac{\gamma_{\rm th}}{\Theta}\Big\} \\
&= \exp\Big(-\frac{\gamma_{\rm th}}{\Phi\Omega_1}\Big) - \exp\Big(-\frac{\gamma_{\rm th}}{\Phi\Omega_1} - \frac{\gamma_{\rm th}}{\Theta\Omega_2}\Big).
\end{aligned} \quad (26)$$

Replacing J_1, J_2, and J_3 in (17), (25), and (26) into (13), we obtain the OP expression of the considered N-WIPT-FDR system as (14) in Theorem 1. The proof is complete.

B. THROUGHPUT

Besides OP, throughput is a crucial parameter for evaluating system performance. In subsection, we derive the closed-form expression of the throughput of the considered N-WIPT-FDR system.

Theorem 2: The throughput (denoted by $\mathcal{T}_{\rm put}$) of the considered N-WIPT-FDR system is given by (27), as shown at the bottom of the next page, where $\mathcal{R}$ is the pre-data transmission rate of the considered system.

$$J_2 = \begin{cases} 0, & \gamma_{\rm th} > \frac{\Phi\Theta}{\Psi} \\ \exp\Big(-\frac{\gamma_{\rm th}}{\Phi\Omega_1} - \frac{\gamma_{\rm th}}{\Theta\Omega_2}\Big) - \exp\Big(-\frac{\Theta}{\Psi\Omega_1} - \frac{\gamma_{\rm th}}{\Theta\Omega_2}\Big) - \frac{\pi}{2N\Omega_1}\Big(\frac{\Theta}{\Psi} - \frac{\gamma_{\rm th}}{\Phi}\Big)\sum_{n=1}^{N}\sqrt{1-\phi_n^2}\exp\Big(-\frac{u}{\Omega_1} - \frac{\gamma_{\rm th}}{\Psi\Omega_2 u}\Big), & \gamma_{\rm th} \leq \frac{\Phi\Theta}{\Psi}. \end{cases} \quad (25)$$

Proof: For the considered N-WIPT-FDR system, since a portion of time α is used for EH, the remaining portion of time used for data exchange is only $1-\alpha$. Thus, the throughput is expressed as

$$\mathcal{T}_{\text{put}} = \mathcal{R}(1-\alpha)(1-\text{OP}), \tag{28}$$

where OP is the outage probability of the considered N-WIPT-FDR system given in (14). Replacing the OP in (14) into (28), we obtain the exact closed-form expression of the throughput as in (27). The proof is complete.

C. AVERAGE SYMBOL ERROR RATE

The ASER the considered N-WIPT-FDR system can be given by [39]

$$\begin{aligned}\text{ASER} &= a\mathbb{E}\{Q(\sqrt{b\gamma_{\text{e2e}}})\} \\ &= \frac{a}{\sqrt{2\pi}}\int_0^\infty F\Big(\frac{t^2}{b}\Big)\exp\Big(-\frac{t^2}{2}\Big)dt,\end{aligned} \tag{29}$$

where (a, b) is a pair whose values depend on the modulation types, e.g., $(a, b) = (2, 1)$ for 4-quadrature amplitude modulation (4-QAM); $(a, b) = (1, 2)$ for the binary phase-shift keying (BPSK) modulation; $Q(x) = \frac{1}{\sqrt{2\pi}}\int_x^\infty e^{-t^2/2}dt$ is the Gaussian function. For the convenience in calculation, we change variable, i.e., $x = \frac{t^2}{b}$, then (29) is rewritten as

$$\text{ASER} = \frac{a\sqrt{b}}{2\sqrt{2\pi}}\int_0^\infty \frac{\exp(-bx/2)}{\sqrt{x}}F(x)dx. \tag{30}$$

From (30), the ASERs of the considered N-WIPT-FDR system is given in the following Theorem 3.

Theorem 3: Under the impacts of nonlinear energy harvester and residual self-interference, the ASER of the considered N-WIPT-FDR system is expressed as (31), as shown at the bottom of the page, where M is the complexity-accuracy trade-off parameter for calculating ASER; $\phi_m = \cos\Big(\frac{(2m-1)\pi}{2M}\Big)$; $w = \frac{\Phi\Theta(1+\phi_m)}{2\Psi}$; $\mathcal{V} = \frac{1}{2}\Big[\frac{\Theta(1+\phi_n)}{\Psi} + \frac{w(1-\phi_n)}{\Phi}\Big]$.

Proof: To derive the ASER of the considered N-WIPT-FDR system from (30), we have to obtain the CDF of γ_{e2e}, which is defined as

$$F(x) = \Pr\{\gamma_{\text{e2e}} < x\}. \tag{32}$$

We can see that (32) is similar to (11). Thus, we can easily obtain $F(x)$ from OP expression by replacing γ_{th} by x. Consequently, $F(x)$ is given by (33), as shown at the bottom of the page, where $v = \frac{1}{2}\Big[\Big(\frac{\Theta}{\Psi} - \frac{x}{\Phi}\Big)\phi_n + \frac{\Theta}{\Psi} + \frac{x}{\Phi}\Big] = \frac{1}{2}\Big[\frac{\Theta(1+\phi_n)}{\Psi} + \frac{x(1-\phi_n)}{\Phi}\Big]$.

Then, ASER is computed as (34), as shown at the bottom of the next page. Now, (34) is rewritten as (35), as shown at the bottom of the next page. For simplicity, we reorganize (35) as (36), as shown at the bottom of the next page. The first line of (36) is calculated by using [40, Eq. (3.361.1)], i.e.,

$$\int_0^\infty \frac{1}{\sqrt{x}}\exp\Big(-\frac{bx}{2}\Big)dx = \sqrt{\frac{2\pi}{b}}, \tag{37}$$

$$\begin{aligned}&\int_0^\infty \frac{1}{\sqrt{x}}\exp\Big(-\frac{bx}{2} - \frac{x}{\Phi\Omega_1} - \frac{x}{\Theta\Omega_2}\Big)dx \\ &= \sqrt{\frac{\pi}{\frac{b}{2} + \frac{1}{\Phi\Omega_1} + \frac{1}{\Theta\Omega_2}}}.\end{aligned} \tag{38}$$

$$\mathcal{T}_{\text{put}} = \begin{cases}\mathcal{R}(1-\alpha)\exp\Big(-\frac{\gamma_{\text{th}}}{\Phi\Omega_1} - \frac{\gamma_{\text{th}}}{\Theta\Omega_2}\Big), & \gamma_{\text{th}} > \frac{\Phi\Theta}{\Psi}, \\ \mathcal{R}(1-\alpha)\Big[\exp\Big(-\frac{\Theta}{\Psi\Omega_1} - \frac{\gamma_{\text{th}}}{\Theta\Omega_2}\Big) + \frac{\pi}{2N\Omega_1}\Big(\frac{\Theta}{\Psi} - \frac{\gamma_{\text{th}}}{\Phi}\Big)\sum_{n=1}^{N}\sqrt{1-\phi_n^2}\exp\Big(-\frac{u}{\Omega_1} - \frac{\gamma_{\text{th}}}{\Psi\Omega_2 u}\Big)\Big], & \gamma_{\text{th}} \le \frac{\Phi\Theta}{\Psi},\end{cases} \tag{27}$$

$$\begin{aligned}\text{ASER} = \frac{a\sqrt{b}}{2\sqrt{2\pi}}\Bigg[&\sqrt{\frac{2\pi}{b}} - \sqrt{\frac{\pi}{\frac{b}{2} + \frac{1}{\Phi\Omega_1} + \frac{1}{\Theta\Omega_2}}} \\ &+ \frac{\pi\Phi\Theta}{2M\Psi}\sum_{m=1}^{M}\sqrt{\frac{1-\phi_m^2}{w}}\exp\Big(-\frac{bw}{2}\Big)\Big(\exp\Big(-\frac{w}{\Phi\Omega_1} - \frac{w}{\Theta\Omega_2}\Big) - \exp\Big(-\frac{w}{\Theta\Omega_2} - \frac{\Theta}{\Psi\Omega_1}\Big)\Big) \\ &- \frac{\pi^2\Phi\Theta}{4MN\Psi\Omega_1}\sum_{m=1}^{M}\sum_{n=1}^{N}\sqrt{(1-\phi_m^2)(1-\phi_n^2)}\Big(\frac{\Theta}{\Psi} - \frac{w}{\Phi}\Big)\exp\Big(-\frac{bw}{2} - \frac{\mathcal{V}}{\Omega_1} - \frac{w}{\Psi\Omega_2\mathcal{V}}\Big)\Bigg]\end{aligned} \tag{31}$$

$$F(x) = \begin{cases}1 - \exp\Big(-\frac{x}{\Phi\Omega_1} - \frac{x}{\Theta\Omega_2}\Big), & x > \frac{\Phi\Theta}{\Psi}, \\ 1 - \exp\Big(-\frac{\Theta}{\Psi\Omega_1} - \frac{x}{\Theta\Omega_2}\Big) - \frac{\pi}{2N\Omega_1}\Big(\frac{\Theta}{\Psi} - \frac{x}{\Phi}\Big)\sum_{n=1}^{N}\sqrt{1-\phi_n^2}\exp\Big(-\frac{v}{\Omega_1} - \frac{x}{\Psi\Omega_2 v}\Big), & x \le \frac{\Phi\Theta}{\Psi},\end{cases} \tag{33}$$

The second line of (36) is solved as (39), as shown at the bottom of the page by using [38, Eq. (25.4.30)], where M, ϕ_m, and v are defined in Theorem 3. Finally, the last line of (36) is calculated by also using [38, Eq. (25.4.30)] to get (40).

$$\begin{aligned}&\int_0^{\frac{\Phi\Theta}{\Psi}} \frac{1}{\sqrt{x}}\Big(\frac{\Theta}{\Psi}-\frac{x}{\Phi}\Big)\exp\Big(-\frac{bx}{2}-\frac{v}{\Omega_1}-\frac{x}{\Psi\Omega_2 v}\Big)dx\\ &=\frac{\pi\Phi\Theta}{2M\Psi}\sum_{m=1}^{M}\sqrt{\frac{1-\phi_m^2}{w}}\Big(\frac{\Theta}{\Psi}-\frac{w}{\Phi}\Big)\\ &\quad\times\exp\Big(-\frac{bw}{2}-\frac{\mathcal{V}}{\Omega_1}-\frac{w}{\Psi\Omega_2\mathcal{V}}\Big).\end{aligned}\tag{40}$$

Replacing (37), (38), (39), and (40) into (36), we obtain the ASER of the considered N-WIPT-FDR system as (31). The proof is complete.

IV. NUMERICAL RESULTS

In this section, we use the expressions of OP and throughput in the previous section to analyze the system performance. The impacts of various parameters such as the saturation power threshold P_{th}, the time switching ratio α, the RSI level k, and the data transmission rate $\mathcal{R}$ on the OP and throughput are deeply investigated. Monte-Carlo simulations are conducted to validate our mathematical analysis. In all results, we set the average SNR as the ratio of the transmission power

$$\begin{aligned}\text{ASER}=\frac{a\sqrt{b}}{2\sqrt{2\pi}}\Bigg[&\int_0^{\frac{\Phi\Theta}{\Psi}}\frac{\exp(-bx/2)}{\sqrt{x}}\Big(1-\exp\Big(-\frac{\Theta}{\Psi\Omega_1}-\frac{x}{\Theta\Omega_2}\Big)-\frac{\pi}{2N\Omega_1}\Big(\frac{\Theta}{\Psi}-\frac{x}{\Phi}\Big)\sum_{n=1}^{N}\sqrt{1-\phi_n^2}\exp\Big(-\frac{v}{\Omega_1}-\frac{x}{\Psi\Omega_2 v}\Big)\Big)\\&+\int_{\frac{\Phi\Theta}{\Psi}}^{\infty}\frac{\exp(-bx/2)}{\sqrt{x}}\Big(1-\exp\Big(-\frac{x}{\Phi\Omega_1}-\frac{x}{\Theta\Omega_2}\Big)\Big)\Bigg].\end{aligned}\tag{34}$$

$$\begin{aligned}\text{ASER}=\frac{a\sqrt{b}}{2\sqrt{2\pi}}\Bigg[&\int_0^{\infty}\frac{1}{\sqrt{x}}\exp\Big(-\frac{bx}{2}\Big)dx-\int_0^{\frac{\Phi\Theta}{\Psi}}\frac{1}{\sqrt{x}}\exp\Big(-\frac{bx}{2}-\frac{\Theta}{\Psi\Omega_1}-\frac{x}{\Theta\Omega_2}\Big)dx\\&-\frac{\pi}{2N\Omega_1}\sum_{n=1}^{N}\sqrt{1-\phi_n^2}\int_0^{\frac{\Phi\Theta}{\Psi}}\frac{1}{\sqrt{x}}\Big(\frac{\Theta}{\Psi}-\frac{x}{\Phi}\Big)\exp\Big(-\frac{bx}{2}-\frac{v}{\Omega_1}-\frac{x}{\Psi\Omega_2 v}\Big)dx\\&-\Big(\int_0^{\infty}\frac{1}{\sqrt{x}}\exp\Big(-\frac{bx}{2}-\frac{x}{\Phi\Omega_1}-\frac{x}{\Theta\Omega_2}\Big)-\int_0^{\frac{\Phi\Theta}{\Psi}}\frac{1}{\sqrt{x}}\exp\Big(-\frac{bx}{2}-\frac{x}{\Phi\Omega_1}-\frac{x}{\Theta\Omega_2}\Big)\Big)\Bigg].\end{aligned}\tag{35}$$

$$\begin{aligned}\text{ASER}=\frac{a\sqrt{b}}{2\sqrt{2\pi}}\Bigg[&\int_0^{\infty}\frac{1}{\sqrt{x}}\exp\Big(-\frac{bx}{2}\Big)dx-\int_0^{\infty}\frac{1}{\sqrt{x}}\exp\Big(-\frac{bx}{2}-\frac{x}{\Phi\Omega_1}-\frac{x}{\Theta\Omega_2}\Big)dx\\&+\int_0^{\frac{\Phi\Theta}{\Psi}}\frac{1}{\sqrt{x}}\exp\Big(-\frac{bx}{2}\Big)\Big(\exp\Big(-\frac{x}{\Phi\Omega_1}-\frac{x}{\Theta\Omega_2}\Big)-\exp\Big(-\frac{\Theta}{\Psi\Omega_1}-\frac{x}{\Theta\Omega_2}\Big)\Big)dx\\&-\frac{\pi}{2N\Omega_1}\sum_{n=1}^{N}\sqrt{1-\phi_n^2}\int_0^{\frac{\Phi\Theta}{\Psi}}\frac{1}{\sqrt{x}}\Big(\frac{\Theta}{\Psi}-\frac{x}{\Phi}\Big)\exp\Big(-\frac{bx}{2}-\frac{v}{\Omega_1}-\frac{x}{\Psi\Omega_2 v}\Big)dx\Bigg].\end{aligned}\tag{36}$$

$$\begin{aligned}&\int_0^{\frac{\Phi\Theta}{\Psi}}\frac{1}{\sqrt{x}}\exp\Big(-\frac{bx}{2}\Big)\Big(\exp\Big(-\frac{x}{\Phi\Omega_1}-\frac{x}{\Theta\Omega_2}\Big)-\exp\Big(-\frac{\Theta}{\Psi\Omega_1}-\frac{x}{\Theta\Omega_2}\Big)\Big)dx\\&=\frac{\pi\Phi\Theta}{2M\Psi}\sum_{m=1}^{M}\sqrt{\frac{1-\phi_m^2}{w}}\exp\Big(-\frac{bw}{2}\Big)\Big(\exp\Big(-\frac{w}{\Phi\Omega_1}-\frac{w}{\Theta\Omega_2}\Big)-\exp\Big(-\frac{w}{\Theta\Omega_2}-\frac{\Theta}{\Psi\Omega_1}\Big)\Big).\end{aligned}\tag{39}$$

TABLE 1. Parameter settings used in evaluating the system performance.

Notation	Description	Fixed value	Varying range
SNR	Signal-to-noise ratio	20 dB	20, 30, 40, 50 dB; $0 \sim 50$ dB
P_{th}/σ^2	Saturation power threshold	30 dB	5, 10, 20, 40, 50 dB
σ^2	Variance of Gaussian noise	1	none
$\mathcal{R}$	Pre-data transmission rate	1 bit/s/Hz	0.5, 1.5, 2, 3, 4 bit/s/Hz
η	Energy harvesting efficiency	0.85	none
α	Time switching ratio	0.5	$0.1 \sim 0.9$
k	RSI level	-30 dB	-20, -10, -5 dB
M, N	Trade-off parameters	50	none

of S to the variance of Gaussian noise, i.e., $\text{SNR} = P_{\text{S}}/\sigma^2$, where $\sigma^2 = \sigma_{\text{R}}^2 = \sigma_{\text{D}}^2$. It is worth noticing that with the parameter settings, the terms Φ and Ψ can be presented via SNR as $\Phi = \frac{P_{\text{S}}}{\gamma_{\text{RSI}}+\sigma_{\text{R}}^2} = \frac{P_{\text{S}}/\sigma_{\text{R}}^2}{(\gamma_{\text{RSI}}/\sigma_{\text{R}}^2)+1} = \frac{\text{SNR}}{(\gamma_{\text{RSI}}/\sigma_{\text{R}}^2)+1}$ and $\Psi = \frac{\eta\alpha P_{\text{S}}}{\sigma_{\text{D}}^2(1-\alpha)} = \frac{\eta\alpha P_{\text{S}}/\sigma_{\text{D}}^2}{1-\alpha} = \frac{\eta\alpha\text{SNR}}{1-\alpha}$. In addition, using the first case of (4) (i.e., $P_{\text{S}} \leq P_{\text{th}}$), Φ can be represented as $\Phi = \frac{\text{SNR}(1-\alpha)}{k\eta\alpha\text{SNR}+1-\alpha}$. As the result, the impacts of the average SNR on the OP, throughput, and ASER of the considered N-WIPT-FDR system are implicitly the impacts of source's transmission power. The energy conversion efficiency is $\eta = 0.85$. In addition, we also simulate the performance of the WIPT-FDR system with a linear harvester to compare with that of the N-WIPT-FDR system. For clarity, the parameter settings for evaluating the system performance are summarized in Table 1.

Fig. 3 plots the OP of the considered N-WIPT-FDR system as a function of the average SNR. We also provide the performance of N-WIPT-FDR and L-WIPT-FDR systems with AF protocol. Herein, various saturation power threshold is investigated, i.e., $P_{\text{th}}/\sigma^2 = 5, 10, 20, 30$ dB. The RSI level is $k = -30$ dB and the time switching ratio is $\alpha = 0.5$. We set $\text{R} = 0.5$ bit/s/Hz for Fig. 3. The analysis curves are plotted using (14) while markers denote Monte-Carlo simulation results. It is obvious that nonlinear energy harvester has a strong effect on the OP of the considered N-WIPT-FDR system. The combined influence of nonlinear energy harvester and the RSI induced by FD transmission causes saturated floor of OP. In particular, the outage floors $\text{OP} = 3 \times 10^{-1}$ and $\text{OP} = 10^{-1}$ corresponding with $P_{\text{th}}/\sigma^2 = 5$ dB and $P_{\text{th}}/\sigma^2 = 10$ dB, respectively, occur at $\text{SNR} = 25$ dB. Therefore, based on this observation, we should use low transmission power of source ($\text{SNR} < 25$ dB) to avoid the waste of energy. For higher saturation power threshold, the outage floor is lower, i.e., $\text{OP} \approx 10^{-2}$ and $\text{OP} \approx 10^{-3}$ corresponding with $P_{\text{th}}/\sigma^2 = 20$ dB and $P_{\text{th}}/\sigma^2 = 30$ dB, respectively. Furthermore, when $\text{SNR} < 35$ dB, the OP of N-WIPT-FDR system with $P_{\text{th}}/\sigma^2 = 30$ dB is similar to that of L-WIPT-FDR system. However, for higher SNR, e.g., $\text{SNR} \geq 35$ dB, the OP of N-WIPT-FDR system is saturated while the OP of the L-WIPT-FDR system still reduces. It is also noted that, due to the effect of RSI, the OP of L-WIPT-FDR system also goes to outage floor in high SNR regime, but this outage floor is lower than that of N-WIPT-FDR system. On the other hand, due to the noise amplification in AF protocol, the DF-based relay systems offer better performance compared with that of AF-based relay system, especially in low SNR regime. In high SNR regime, due to the error floors are appears, the performance of both AF and DF protocols are similar.

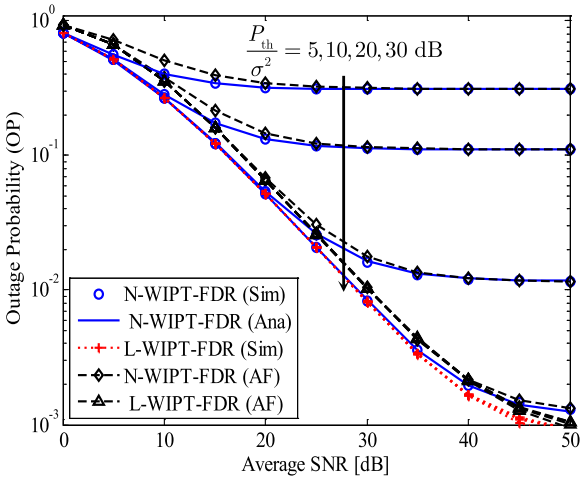

FIGURE 3. The OP of the considered N-WIPT-FDR system versus the average SNR for various saturation power threshold, i.e., $P_{\text{th}}/\sigma^2 = 10, 20, 30, 50$ dB, the RSI level $k = -30$ dB, the EH time duration $\alpha = 0.5$ and the pre-data transmission rate $\text{R} = 0.5$ bit/s/Hz.

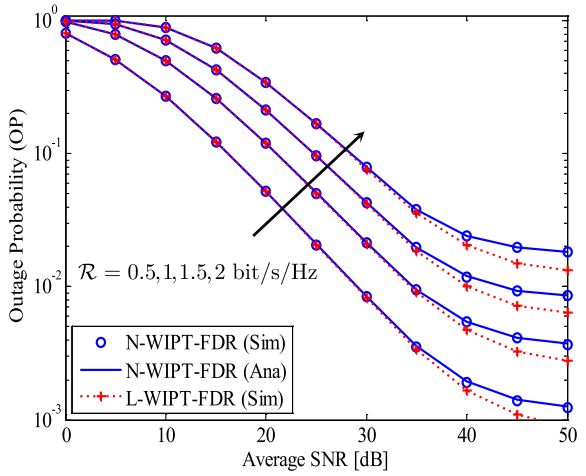

FIGURE 4. The OP of the considered N-WIPT-FDR system for different data transmission rates with $P_{\text{th}}/\sigma^2 = 30$ dB.

Fig. 4 illustrates the effect of data transmission rates on the OP of the considered N-WIPT-FDR system with $P_{\text{th}}/\sigma^2 = 30$ dB. Other parameters for obtaining Fig. 4 are similar to those used in Fig. 3. As can be seen from Fig. 4, a higher data transmission rate leads to higher OP. In particular, for low data transmission rate, e.g., $\mathcal{R} = 0.5$ bit/s/Hz, the OP of N-WIPT-FDR system can reach 10^{-3} at $\text{SNR} = 50$ dB. Meanwhile, it is 4×10^{-3} at $\text{SNR} = 50$ dB for

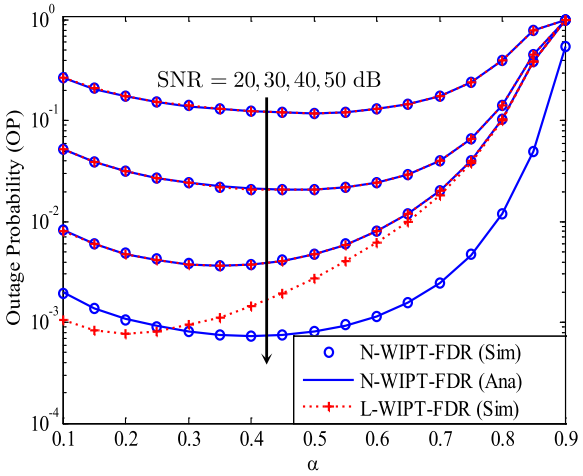

FIGURE 5. The OP of the considered N-WIPT-FDR system versus the time switching ratio α for different values of SNR, $P_{\text{th}}/\sigma^2 = 40$ dB.

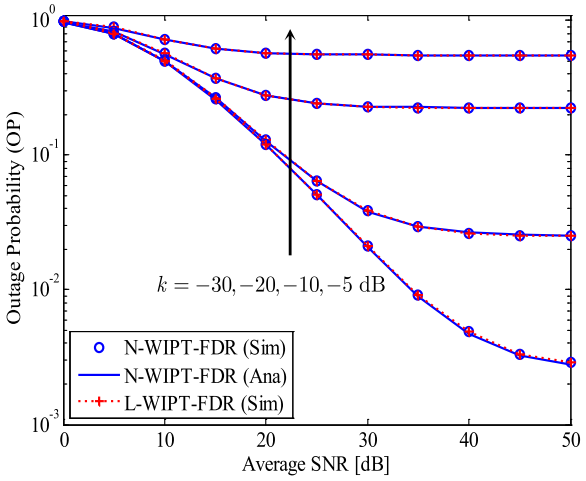

FIGURE 6. The effect of RSI level on the OP of the considered N-WIPT-FDR system for $P_{\text{th}}/\sigma^2 = 50$ dB.

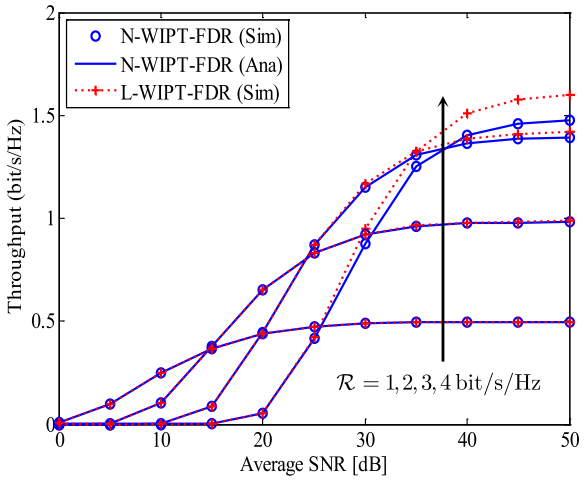

FIGURE 7. The throughput of the considered N-WIPT-FDR system for different data transmission rates, $k = -30$ dB, $P_{\text{th}}/\sigma^2 = 30$ dB.

$\mathcal{R} = 1$ bit/s/Hz. When the data transmission rate increases, the OP also increases. For example, for $\mathcal{R} = 2$ bit/s/Hz, the OP is only approximately 10^{-2} at SNR $= 50$ dB. On the other hand, when the transmission power of the source is less than the saturation power threshold of nonlinear harvester (SNR < 30 dB), the OPs of N-WIPT-FDR and L-WIPT-FDR systems are similar. Otherwise, the OP of the N-WIPT-FDR system is significantly higher than that of the L-WIPT-FDR system due to the nonlinear characteristic of the harvested energy.

Fig. 5 considers the OP of N-WIPT-FDR system versus the time switching ratio α for different values of SNR. We see that the impact of α on the OP is remarkably different for each value of SNR. Furthermore, for a certain SNR, there is an optimal value of α that minimizes the OP of the N-WIPT-FDR system, and this value is decreased with the increase of SNR. Specifically, the optimal α corresponding to SNR $= 20, 30$, and 40 dB are 0.5, 0.45, and 0.35, respectively. The L-WIPT-FDR system behaves similarly. It is because these SNRs (20, 30, 40 dB) are not higher than the saturation power threshold (40 dB). However, when SNR $= 50$ dB, the optimal α is 0.4 for the N-WIPT-FDR system but is 0.2 for L-WIPT-FDR system. These results significantly reflect the characteristics of N-WIPT-FDR and L-WIPT-FDR systems as the SNR is much higher than the saturation power threshold nonlinear energy harvester, i.e., $P_{\text{S}}|h_{\text{SR}}|^2 \gg P_{\text{th}}$. In summary, when we increase the source's transmission power, the optimal α of the L-WIPT-FDR system is decreased. However, for the considered N-WIPT-FDR system, besides depending on the source's transmission power, the optimal α also depends on the saturation power threshold of the nonlinear energy harvester.

Fig. 6 investigates the effect of RSI level on the OP of the considered N-WIPT-FDR system. To clearly show the effect of the RSI level, we choose $P_{\text{th}}/\sigma^2 = 50$ dB. For this value of the saturation power threshold, the OPs of N-WIPT-FDR and L-WIPT-FDR systems are almost similar. We can see in Fig. 6 that the RSI level has a great effect on the OP of the N-WIPT-FDR system. Specifically, when $k = -5$ and -10 dB, the OP slowly decreases and reaches the error floor quickly with OP $= 5 \times 10^{-1}$ and 2×10^{-1}, respectively, at SNR $= 30$ dB. When the RSI level is lower, e.g., $k = -20$ dB, OP still goes to the error floor but with significantly lower value, i.e., at SNR $= 40$ dB, OP $= 2.6 \times 10^{-2}$ for $k = -20$ dB while OP $= 2 \times 10^{-1}$ for $k = -10$ dB. When the RSI level is even smaller, e.g., $k = -30$ dB, the OP rapidly decreases as SNR increases. Also, the OP does not go to the error floor in the considered SNR range. These results demonstrate the importance of SIC techniques to FD communication. Therefore, more efforts need to be put on SIC at FD devices to enhance FD communication systems' performance, making them technically feasible.

Fig. 7 illustrates the throughput of the considered N-WIPT-FDR system for different data transmission rates, $k = -30$ dB, $P_{\text{th}}/\sigma^2 = 30$ dB. Other parameters used to obtain Fig. 7 are similar to those used in Fig. 3. Because

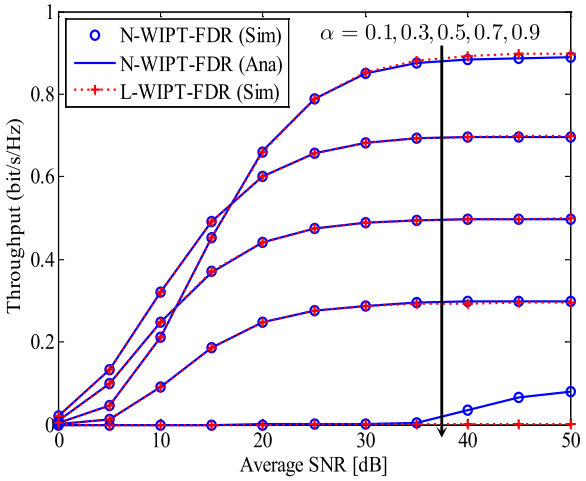

FIGURE 8. The effect of time switching ratio α on the throughput of the considered N-WIPT-FDR system, $k = -30$ dB, $P_{\text{th}}/\sigma^2 = 30$ dB, $\mathcal{R} = 1$ bit/s/Hz.

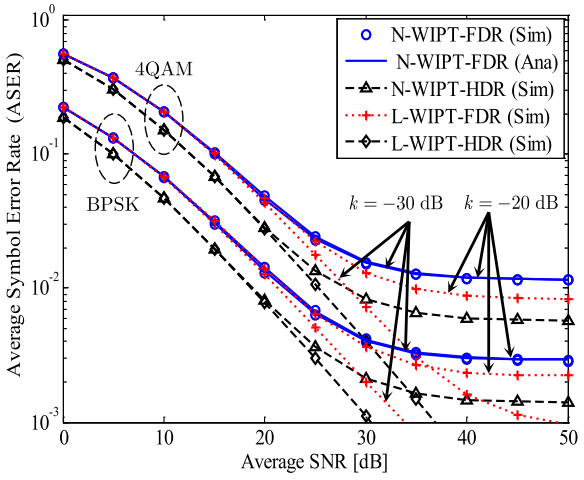

FIGURE 9. The ASERs of the considered N-WIPT-FDR system for two modulation schemes and two RSI levels in comparison with the ASERs of N-WIPT-HDR system, $P_{\text{th}}/\sigma^2 = 20$ dB.

only half of a symbol period is used for EH ($\alpha = 0.5$), the throughput of the N-WIPT-FDR system cannot reach the target throughput. For examples, when $\mathcal{R} = 1$ and $\mathcal{R} = 2$ bit/s/Hz, the throughput of N-WIPT-FDR system respectively reaches 0.5 and 1 bit/s/Hz at SNR = 40 dB. When higher data transmission rate is used, e.g., $\mathcal{R} = 3$ bit/s/Hz, the throughput is only 1.4 bit/s/Hz at SNR = 50 dB. Especially, when $\mathcal{R} = 4$ bit/s/Hz, the throughput is 1.5 bit/s/Hz. To sum up, for low data transmission rates ($\mathcal{R} = 1, 2$ bit/s/Hz), the considered N-WIPT-FDR system can reach half of the target throughput. However, for a high data transmission rate ($\mathcal{R} = 3, 4$ bit/s/Hz), the considered system cannot reach half of the target throughput. Another observation is that the difference between the throughput of N-WIPT-FDR and L-WIPT-FDR systems is significant at high data transmission rates ($\mathcal{R} = 3, 4$ bit/s/Hz). For wireless systems, we want to get high throughput but low OP. Thus, we need to choose suitable values of the system parameters such as $\mathcal{R}$ and α to achieve this target. We see that with high data transmission rates, the OP is also high (refer to Fig. 4). Therefore, we should use low data transmission rates for the considered N-WIPT-FDR system to obtain both low OP and high throughput.

Fig. 8 investigates the throughput of the considered N-WIPT-FDR system for different values of time switching ratio α. Herein, we use $P_{\text{th}}/\sigma^2 = 30$ dB to clearly show the impact of the nonlinear harvester on the throughput in high SNR regime. We see that the throughput of both N-WIPT-FDR and L-WIPT-FDR systems increases when α decreases. This result is reasonable because when α is smaller, the EH time duration is shorter; thus, more time for data transmission is available, resulting in higher throughput. It is also noted that, although we want to get higher throughput of the N-WIPT-FDR system, we should not use small α because small α means the EH time duration is very short, making the relay cannot harvest enough energy for data transmission. Consequently, the end-to-end SINR is low. In this case, the OP of the N-WIPT-FDR system is very high because the destination cannot successfully decode the received signals. To sum up, there is a trade-off between the OP performance and throughput; therefore, we should use a suitable value of α that can balance the OP and throughput of N-WIPT-FDR system. On the other hand, when $\alpha = 0.9$, the throughput of the N-WIPT-FDR system is higher than that of the L-WIPT-FDR system when SNR $>$ 35 dB. This feature is due to the linear and nonlinear characteristics of the energy harvester. Particularly, the transmission power of the FD relay in the L-WIPT-FDR system increases with the transmission power of the source, leading to high RSI at the FD relay. Meanwhile, the FD relay's transmission power in the N-WIPT-FDR system is saturated when SNR $>$ 35 dB, then the value of RSI is also saturated. Therefore, in high SNR regime, the RSI power of the N-WIPT-FDR system is lower than that of the L-WIPT-FDR system, resulting in higher throughput.

Fig. 9 shows the ASERs of the considered N-WIPT-FDR system for two modulation schemes, i.e., BPSK ($(a, b) = (1, 2)$) and 4-QAM ($(a, b) = (2, 1)$) and two RSI levels ($k = -30, -20$ dB) in comparison with the ASERs of N-WIPT-HDR system. We use (31) to obtain the analysis curves of ASERs of the considered N-WIPT-FDR system. It is obvious that for the considered N-WIPT-FDR system, the ASERs with $k = -30$ dB and $k = -20$ dB are similar. However, they are different for L-WIPT-FDR system. Specifically, when 4-QAM is used, ASERs of N-WIPT-FDR system reach the error floor of 10^{-2} for both $k = -30$ dB and $k = -20$ dB. Meanwhile, ASERs of L-WIPT-FDR system reach the error floors of 10^{-3} and 7×10^{-3} when $k = -30$ dB and $k = -20$ dB, respectively. Furthermore, ASER of L-WIPT-FDR system with $k = -30$ dB avoids the error floor in the investigated SNR range. On the other hand, since N-WIPT-FDR system and L-WIPT-FDR system are affected by RSI due to FD mode, the ASERs of them are, respectively,

higher than those of N-WIPT-HDR system and L-WIPT-HDR system.[1] Additionally, N-WIPT-HDR system is also affected by the saturation power threshold. Thus, the ASERs of N-WIPT-HDR system reach the error floor in high SNR regime. In particularly, ASER of L-WIPT-FDR system may be lower or higher than that of N-WIPT-HDR system, depending on the RSI level and transmission power of source. For example, in the case of $k = -30$ dB, when SNR < 30 dB, ASERs of L-WIPT-FDR system are higher than those of N-WIPT-HDR system. However, when SNR > 30 dB, ASERs of L-WIPT-FDR system are lower than those of N-WIPT-HDR system. These features clearly indicate a great impact of nonlinear energy harvester on the performance of N-WIPT-HDR and N-WIPT-FDR system. Therefore, more efforts to reduce the RSI level and nonlinearity in energy harvester should be made in the future to improve the performance of the considered N-WIPT-FDR system.

V. CONCLUSION

Although energy harvesting in FD communication systems has been widely studied, most of the works had focused on linear energy harvester. Meanwhile, nonlinear energy harvester is more practical for wireless communication systems. In this paper, we investigate the case where the FD relay is equipped with nonlinear energy harvester. We successfully derived the exact closed-form expressions of outage probability, throughput, and average symbol error rate of a N-WIPT-FDR system over Rayleigh fading channels. These expressions can be used for analyzing the performance of relevant systems such as L-WIPT-FDR, L-WIPT-HDR, and N-WIPT-HDR systems. We compared the performance of N-WIPT-FDR system with that of L-WIPT-FDR system, N-WIPT-HDR system, and L-WIPT-HDR system in various scenarios. Numerical results showed that the OP, throughput, and ASER of the N-WIPT-FDR system were greatly affected by the saturation power threshold of nonlinear energy harvester, the RSI induced by FD transmission, and the EH time duration. Under the joint impact of the saturation power threshold and RSI, the OP, throughput, and ASER of the considered N-WIPT-FDR system reached the floors in the high SNR regime. Moreover, there is an optimal time switching ratio, which minimizes the OP of the N-WIPT-FDR system. This optimal value depends on the source's transmission power and the nonlinear energy harvester's saturation power threshold. Therefore, by choosing a suitable time switching ratio, we can improve the OP and throughput performance of the N-WIPT-FDR system.

[1]Notice that for HDR system, αT time units is used for EH at relay, $(1-\alpha)T/2$ time units is used for transmitting signal from S to R and $(1-\alpha)T/2$ time units is used for transmitting signal from R to D. As a result, the transmission power at relay in the case of HDR is expressed as

$$P_{\mathrm{R}} = \frac{E_{\mathrm{NEH}}}{(1-\alpha)T/2} = \begin{cases} \frac{2\eta\alpha P_{\mathrm{S}}|h_{\mathrm{SR}}|^2}{1-\alpha}, & P_{\mathrm{S}}|h_{\mathrm{SR}}|^2 \le P_{\mathrm{th}}, \\ \frac{2\eta\alpha P_{\mathrm{th}}}{1-\alpha}, & P_{\mathrm{S}}|h_{\mathrm{SR}}|^2 > P_{\mathrm{th}}. \end{cases} \quad (41)$$

REFERENCES

[1] I. B. Sofi and A. Gupta, "A survey on energy efficient 5G green network with a planned multi-tier architecture," *J. Netw. Comput. Appl.*, vol. 118, pp. 1–28, Sep. 2018.

[2] X. Zhou, R. Zhang, and C. K. Ho, "Wireless information and power transfer: Architecture design and rate-energy tradeoff," *IEEE Trans. Commun.*, vol. 61, no. 11, pp. 4754–4767, Nov. 2013.

[3] B. Clerckx, R. Zhang, R. Schober, D. W. K. Ng, D. I. Kim, and H. V. Poor, "Fundamentals of wireless information and power transfer: From RF energy harvester models to signal and system designs," *IEEE J. Sel. Areas Commun.*, vol. 37, no. 1, pp. 4–33, Jan. 2019.

[4] N. T. Do, D. B. da Costa, T. Q. Duong, V. N. Q. Bao, and B. An, "Exploiting direct links in multiuser multirelay SWIPT cooperative networks with opportunistic scheduling," *IEEE Trans. Wireless Commun.*, vol. 16, no. 8, pp. 5410–5427, Aug. 2017.

[5] B. C. Nguyen and X. N. Tran, "Performance analysis of full-duplex amplify-and-forward relay system with hardware impairments and imperfect self-interference cancellation," *Wireless Commun. Mobile Comput.*, vol. 2019, pp. 1–10, Aug. 2019.

[6] A. H. Gazestani, S. A. Ghorashi, B. Mousavinasab, and M. Shikh-Bahaei, "A survey on implementation and applications of full duplex wireless communications," *Phys. Commun.*, vol. 34, pp. 121–134, Jun. 2019.

[7] B. C. Nguyen, T. M. Hoang, and P. T. Tran, "Improving the performance of spatial modulation full-duplex relaying system with hardware impairment using transmit antenna selection," *IEEE Access*, vol. 8, pp. 20191–20202, 2020.

[8] V. Singh, A. Gadre, and S. Kumar, "Full duplex radios," in *Proc. 19th ACM Workshop Hot Topics Netw.*, vol. 43, no. 4, 2013, pp. 375–386.

[9] M. Heino, D. Korpi, T. Huusari, E. Antonio-Rodriguez, S. Venkatasubramanian, T. Riihonen, L. Anttila, C. Icheln, K. Haneda, R. Wichman, and M. Valkama, "Recent advances in antenna design and interference cancellation algorithms for in-band full duplex relays," *IEEE Commun. Mag.*, vol. 53, no. 5, pp. 91–101, May 2015.

[10] D. Zhai, H. Chen, Z. Lin, Y. Li, and B. Vucetic, "Accumulate then transmit: Multiuser scheduling in full-duplex wireless-powered IoT systems," *IEEE Internet Things J.*, vol. 5, no. 4, pp. 2753–2767, Aug. 2018.

[11] Y. Alsaba, C. Y. Leow, and S. K. Abdul Rahim, "Full-duplex cooperative non-orthogonal multiple access with beamforming and energy harvesting," *IEEE Access*, vol. 6, pp. 19726–19738, 2018.

[12] B. C. Nguyen, T. M. Hoang, and P. T. Tran, "Performance analysis of full-duplex decode-and-forward relay system with energy harvesting over Nakagami-m fading channels," *AEU-Int. J. Electron. Commun.*, vol. 98, pp. 114–122, Jan. 2019.

[13] G. Chen, P. Xiao, J. R. Kelly, B. Li, and R. Tafazolli, "Full-duplex wireless-powered relay in two way cooperative networks," *IEEE Access*, vol. 5, pp. 1548–1558, 2017.

[14] C. Zhong, H. A. Suraweera, G. Zheng, I. Krikidis, and Z. Zhang, "Wireless information and power transfer with full duplex relaying," *IEEE Trans. Commun.*, vol. 62, no. 10, pp. 3447–3461, Oct. 2014.

[15] B. C. Nguyen, T. M. Hoang, P. T. Tran, and T. N. Nguyen, "Outage probability of NOMA system with wireless power transfer at source and full-duplex relay," *AEU-Int. J. Electron. Commun.*, vol. 116, Mar. 2020, Art. no. 152957.

[16] D.-H. Chen and Y.-C. He, "Full-duplex secure communications in cellular networks with downlink wireless power transfer," *IEEE Trans. Commun.*, vol. 66, no. 1, pp. 265–277, Jan. 2018.

[17] B. C. Nguyen, T. M. Hoang, X. N. Pham, and P. T. Tran, "Performance analysis of energy harvesting-based full-duplex decode-and-forward vehicle-to-vehicle relay networks with nonorthogonal multiple access," *Wireless Commun. Mobile Comput.*, vol. 2019, pp. 1–11, Nov. 2019.

[18] A. Koc, I. Altunbas, and E. Basar, "Two-way full-duplex spatial modulation systems with wireless powered AF relaying," *IEEE Wireless Commun. Lett.*, vol. 7, no. 3, pp. 444–447, Jun. 2018.

[19] J. Li, L. C. Tran, and F. Safaei, "Outage probability and throughput analyses in full-duplex relaying systems with energy transfer," *IEEE Access*, vol. 8, pp. 150150–150161, 2020.

[20] K. Agrawal, S. Prakriya, and M. F. Flanagan, "Optimization of SWIPT with battery-assisted energy harvesting full-duplex relays," *IEEE Trans. Green Commun. Netw.*, early access, Nov. 3, 2020, doi: 10.1109/TGCN.2020.3035621.

[21] T. M. Hoang, X. N. Tran, B. C. Nguyen, and L. T. Dung, "On the performance of MIMO full-duplex relaying system with SWIPT under outdated CSI," *IEEE Trans. Veh. Technol.*, vol. 69, no. 12, pp. 15580–15593, Dec. 2020.
[22] K. Agrawal, M. F. Flanagan, and S. Prakriya, "NOMA with battery-assisted energy harvesting full-duplex relay," *IEEE Trans. Veh. Technol.*, vol. 69, no. 11, pp. 13952–13957, Nov. 2020.
[23] Q. N. Le, A. Yadav, N. P. Nguyen, O. A. Dobre, and R. Zhao, "Full-duplex non-orthogonal multiple access cooperative overlay spectrum-sharing networks with SWIPT," *IEEE Trans. Green Commun. Netw.*, early access, Nov. 5, 2020, doi: 10.1109/TGCN.2020.3036026.
[24] S. A. A. Kazmi and S. Coleri, "Optimization of full-duplex relaying system with non-linear energy harvester," *IEEE Access*, vol. 8, pp. 201566–201576, 2020.
[25] L. Zheng, D. Liu, Z. Wen, and J. Zou, "Robust beamforming for multi-user MISO full-duplex SWIPT system under non-linear energy harvesting model," *IEEE Access*, vol. 9, pp. 14387–14397, 2021.
[26] E. Boshkovska, D. W. K. Ng, N. Zlatanov, and R. Schober, "Practical non-linear energy harvesting model and resource allocation for SWIPT systems," *IEEE Commun. Lett.*, vol. 19, no. 12, pp. 2082–2085, Dec. 2015.
[27] Y. Dong, M. J. Hossain, and J. Cheng, "Performance of wireless powered amplify and forward relaying over Nakagami- fading channels with non-linear energy harvester," *IEEE Commun. Lett.*, vol. 20, no. 4, pp. 672–675, Apr. 2016.
[28] Z. Wei, S. Sun, X. Zhu, D. In Kim, and D. W. K. Ng, "Resource allocation for wireless-powered full-duplex relaying systems with nonlinear energy harvesting efficiency," *IEEE Trans. Veh. Technol.*, vol. 68, no. 12, pp. 12079–12093, Dec. 2019.
[29] K. Xu, M. Zhang, J. Liu, N. Sha, W. Xie, and L. Chen, "SWIPT in mMIMO system with non-linear energy-harvesting terminals: Protocol design and performance optimization," *EURASIP J. Wireless Commun. Netw.*, vol. 2019, no. 1, pp. 1–15, Dec. 2019.
[30] K. Xu, Z. Shen, M. Zhang, Y. Wang, X. Xia, W. Xie, and D. Zhang, "Beam-domain SWIPT for mMIMO system with nonlinear energy harvesting legitimate terminals and a non-cooperative terminal," *IEEE Trans. Green Commun. Netw.*, vol. 3, no. 3, pp. 703–720, Sep. 2019.
[31] M. Babaei, U. Aygolu, M. Basaran, and L. Durak-Ata, "BER performance of full-duplex cognitive radio network with nonlinear energy harvesting," *IEEE Trans. Green Commun. Netw.*, vol. 4, no. 2, pp. 448–460, Jun. 2020.
[32] K. M. Rabie, B. Adebisi, and M.-S. Surname, "Half-duplex and full-duplex AF and DF relaying with energy-harvesting in log-normal fading," *IEEE Trans. Green Commun. Netw.*, vol. 1, no. 4, pp. 468–480, Dec. 2017.
[33] A. Sabharwal, P. Schniter, D. Guo, D. W. Bliss, S. Rangarajan, and R. Wichman, "In-band full-duplex wireless: Challenges and opportunities," *IEEE J. Sel. Areas Commun.*, vol. 32, no. 9, pp. 1637–1652, Sep. 2014.
[34] E. Ahmed and A. M. Eltawil, "All-digital self-interference cancellation technique for full-duplex systems," *IEEE Trans. Wireless Commun.*, vol. 14, no. 7, pp. 3519–3532, Jul. 2015.
[35] C. Li, B. Xia, S. Shao, Z. Chen, and Y. Tang, "Multi-user scheduling of the full-duplex enabled two-way relay systems," *IEEE Trans. Wireless Commun.*, vol. 16, no. 2, pp. 1094–1106, Feb. 2017.
[36] B. C. Nguyen, X. N. Tran, D. T. Tran, X. N. Pham, and L. T. Dung, "Impact of hardware impairments on the outage probability and ergodic capacity of one-way and two-way full-duplex relaying systems," *IEEE Trans. Veh. Technol.*, vol. 69, no. 8, pp. 8555–8567, Aug. 2020.
[37] L. Van Nguyen, B. C. Nguyen, X. N. Tran, and L. T. Dung, "Transmit antenna selection for full-duplex spatial modulation multiple-input multiple-output system," *IEEE Syst. J.*, vol. 14, no. 4, pp. 4777–4785, Dec. 2020.
[38] M. Abramowitz and I. A. Stegun, *Handbook of Mathematical Functions: With Formulas, Graphs, and Mathematical Tables*, vol. 9. New York, NY, USA: Dover, 1972.
[39] A. Goldsmith, *Wireless Communications*. Cambridge, U.K.: Cambridge Univ. Press, 2005.
[40] A. Jeffrey and D. Zwillinger, *Table of Integrals, Series, and Products*. New York, NY, USA: Academic, 2007.

BA CAO NGUYEN received the B.S. degree from Telecommunications University, Khanh Hoa, Vietnam, in 2006, the M.S. degree from the Posts and Telecommunications Institute of Technology (VNPT), Ho Chi Minh City, Vietnam, in 2011, and the Ph.D. degree from Le Quy Don Technical University, Hanoi, Vietnam, in 2020. He is currently a Lecturer with Telecommunications University. His research interests include energy harvesting, full-duplex, spatial modulation, NOMA, MIMO, and cooperative communication.

TRAN MANH HOANG received the B.S. degree in communication command from Telecommunications University, Ministry of Defense, Khanh Hoa, Vietnam, in 2002, the B.Eng. degree in electrical engineering from Le Quy Don Technical University, Hanoi, Vietnam, in 2006, the M.Eng. degree in electronics engineering from Posts and Telecommunications Institute of Technology, Ho Chi Minh City, Vietnam, in 2013, and the Ph.D. degree from Le Quy Don Technical University, Hanoi, Vietnam, in 2020. He is currently a Lecturer with Telecommunications University. His research interests include energy harvesting, non-orthogonal multiple access, and signal processing for wireless cooperative communications.

LE THE DUNG (Member, IEEE) received the B.S. degree in electronics and telecommunication engineering from Ho Chi Minh City University of Technology, Ho Chi Minh City, Vietnam, in 2008, and the M.S. and Ph.D. degrees in electronics and computer engineering from Hongik University, Seoul, South Korea, in 2012 and 2016, respectively. From 2007 to 2010, he joined Signet Design Solutions Vietnam, as a Hardware Design Engineer. Since May 2016, he has been with Chungbuk National University, as a Postdoctoral Research Fellow. He has more than 60 papers in refereed international journals and conferences. His major research interests include routing protocols, network coding, network stability analysis, optimization in mobile ad-hoc networks, cognitive radio ad-hoc networks, and visible light communication networks. He was a recipient of the IEEE IS3C2016 Best Paper Award.

TAEJOON KIM (Member, IEEE) received the B.S. degree in electronics engineering from Yonsei University, Seoul, Republic of Korea, in 2003, and the Ph.D. degree in electrical engineering from the Korea Advanced Institute of Science and Technology (KAIST), Daejeon, Republic of Korea, in 2011. From 2003 to 2005, he was a Researcher with LG Electronics, Seoul. From 2011 to 2013, he was a Senior Researcher with the Electronics and Telecommunications Research Institute (ETRI), Daejeon. His research interests include communication theory and analysis and optimization of wireless networks.